Computational Materials Science 157 (2019) 168–174

Contents lists available at ScienceDirect

Computational Materials Science

journal homepage: www.elsevier.com/locate/commatsci

Nanoindentation of monolayer $Ti_{n+1}C_nT_x$ MXenes via atomistic simulations: The role of composition and defects on strength

Gabriel Plummer[a,b], Babak Anasori[a], Yury Gogotsi[a], Garritt J. Tucker[a,b,*]

[a] Department of Materials Science and Engineering, and A.J. Drexel Nanomaterials Institute, Drexel University, Philadelphia, PA 19104, USA
[b] Department of Mechanical Engineering, Colorado School of Mines, Golden, CO 80401, USA

ARTICLE INFO

Keywords:
MXenes
Nanoindentation
Atomistic simulations
ReaxFF

ABSTRACT

Since their discovery in 2011, interest in MXenes, two-dimensional transition metal carbides and/or nitrides, has greatly expanded due to their promising functional properties and facile synthesis methods, and their development for emerging technologies is propitiously progressing. Despite promising advancements, there still remains a lack of understanding with regards to their fundamental mechanical properties. Here, nanoindentation of the $Ti_{n+1}C_nT_x$ MXenes was studied via atomistic simulations utilizing a parametrization of the ReaxFF interatomic potential, to understand the influence of point defects. From force-displacement curves, the Young's moduli of pristine $Ti_3C_2O_2$ and Ti_2CO_2 were calculated to be 466 GPa and 983 GPa, respectively. The influence of both titanium and carbon vacancies (V_{Ti} and V_C) on $Ti_3C_2O_2$ were also quantified using simulated nanoindentation of a set of samples containing both 1% V_{Ti} and 10% V_C, resulting in a reduction of the calculated Young's modulus to 386 ± 31 GPa. Of particular importance, is that these results mirror recent experimental findings indicating the fundamental role of defects in the mechanical behavior of MXenes. The calculated modulus in this work for the defect-containing $Ti_3C_2O_2$ surpasses that of graphene oxide, establishing it as a new benchmark in strength for solution-processed, 2D materials. Results here also indicate improvements can be made in current MXene processing methods to better approach the theoretical strength of pristine 2D materials.

1. Introduction

The family of 2D materials was significantly expanded in 2011 with the discovery of MXenes [1], a group of early transition metal carbides and/or nitrides which take on the chemical formula $M_{n+1}X_nT_x$. M is an early transition metal, X is either carbon or nitrogen, T represents surface terminations of −O, −OH, or −F, and n = 1, 2, or 3. They are composed of alternating layers of M and X elements (Fig. 1c). The majority of MXenes are derived from their MAX precursors when the A-element in a MAX phase is selectively etched with a fluoride-containing acidic solution [2]. There are close to 100 MAX phases available and hundreds of MAX phases can be made in the form of mono-transition metal or multiple transition metal carbides and nitrides in the forms of solid solutions or ordered phases [2–4]. To date, there have been close to 30 MXenes synthesized, and the fundamental properties of several additional MXene compositions have been studied theoretically [2,5]. MXenes have been explored for use in many of the applications in which other 2D materials have been envisioned, and in some applications, such as energy storage and electromagnetic interference shielding, MXenes have outperformed other 2D materials [2,6,7]. Significant focus on studying their electronic and electrochemical storage properties has led to substantial innovations and developments, but critically, there is still a relative lack of understanding of their fundamental mechanical properties.

The mechanical properties of 2D materials are of great interest as they have been shown to be vastly different than their bulk counterparts owing to the limited length-scale in the nano regime. Graphene has been experimentally measured to have a Young's modulus of 1 TPa [8], making it the strongest known material. Early density functional theory (DFT) calculations indicate MXenes have similarly favorable mechanical properties with Young's moduli ranging from 500 to 800 GPa, and all are predicted to be stronger than their parent MAX phases [9]. While MXenes may not reach the impressive strength attained by graphene, they do have a distinct advantage in processing. Graphene must be mechanically exfoliated from graphite, a tedious and inefficient process resulting in only small amounts of 2D material when single-layer flakes are made [10]. MXenes, however, are processed in solution providing two distinct advantages: (1) larger quantities produced at a single time, and (2) the terminations imparted by the solution create a hydrophilic surface allowing for easy incorporation into

* Corresponding author at: Department of Mechanical Engineering, Colorado School of Mines, Golden, CO 80401, USA.
E-mail address: tucker@mines.edu (G.J. Tucker).

https://doi.org/10.1016/j.commatsci.2018.10.033
Received 28 August 2018; Received in revised form 23 October 2018; Accepted 27 October 2018
Available online 08 November 2018
0927-0256/

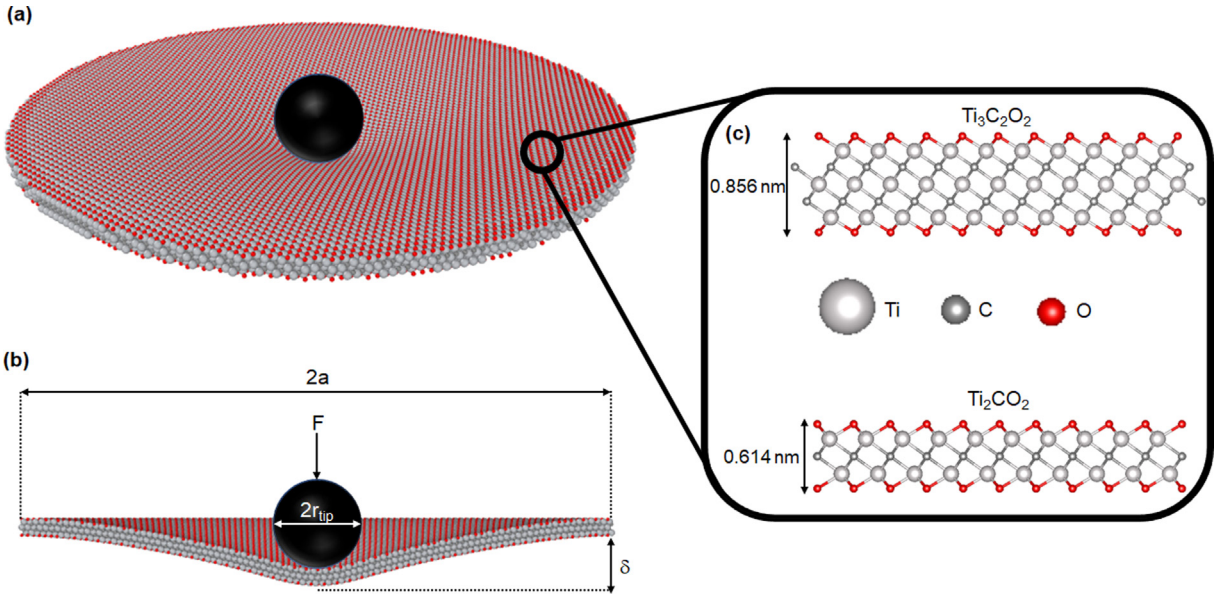

Fig. 1. Indentation schematic showing (a) a perspective view of a MXene monolayer being indented with a spherical indenter tip, (b) a cross-sectional view giving the relevant dimensions for Eqs. (2) and (3), and (c) the intralayer structure of $Ti_3C_2O_2$ and Ti_2CO_2 MXenes.

polymer-based composites [2,11–14], similar to graphene oxide. By comparison, when graphene is solution-processed, the result is graphene oxide with a significantly reduced Young's modulus of 200 GPa [15] compared to pure graphene. As such, MXenes, have the potential to become a new benchmark in strength for solution-processed 2D materials.

The most studied MXene, $Ti_3C_2T_x$, has been demonstrated to be useful in a variety of applications in which mechanical properties are paramount. Structural composites with a MXene nanofiller in polymer matrices exhibit significantly enhanced tensile strength compared to each individual component [11,16]. Among the most studied applications for MXenes are electrodes in energy storage devices [2] - operating on the principle of ion intercalation. This process may result in significant diffusion-induced stresses in the electrode upon cycling [17]. Due to the stresses introduced, a mechanically robust material is required in order to withstand large numbers of cycles while maintaining its favorable initial atomic structure. Composite films consisting of $Ti_3C_2T_x$ MXenes, carbon nanotubes (CNTs), and polymer fibers have been incorporated into energy storage devices and exhibit exceptional tolerance to repeated deformation without failure [18,19]. Additionally, water desalination and purification membranes [20–23], as well as gas separation membranes made of MXene [24] will require high mechanical strength to withstand the pressure during filtration. Another application being explored for MXenes is piezoresistive sensors for wearable electronics. Sensors utilizing both $Ti_3C_2T_x$ MXene alone [25] as well as a layered MXene/CNT composite [26] have successfully detected both small and large deformations with high sensitivity and excellent stability. These technological applications show the great potential for MXenes in a variety of emerging areas. A further characterization of their fundamental mechanical properties will help provide a better understanding of their limits in these applications and will help inversely guide new directions for their implementation.

While a plethora of mechanical testing methods exist for bulk-level characterization of materials, translation of these approaches to 2D materials has remained challenging – indentation is one exception. First demonstrated by Lee et al. with graphene [8], indentation employs an atomic force microscope (AFM) to apply force at the center of a film of 2D material suspended over a substrate with circular holes. Based on success with graphene, indentation has become the standard for mechanical testing of 2D materials, and its application to other materials such as graphene oxide [15], h-BN [27], and MoS_2 [28] has followed. It is clear that indentation has the potential to characterize MXenes, and due to recent advances in the synthesis of $Ti_3C_2T_x$ [29], the first experimental measurements of its elastic properties have now been made via AFM indentation [30]. Lipatov et al. measured a number of monolayer samples, and the Young's modulus was calculated to be 330 ± 30 GPa [30]. While this measured value is lower than the Young's modulus predicted in previous DFT [9] and molecular dynamics (MD) [31] studies, it has still been established as the new benchmark for strength in solution-processed, 2D materials, surpassing graphene oxide.

Computational methods have been instrumental thus far in developing a better understanding of MXene structures and properties, acting as a guide for experimental efforts [5] and providing insight into MXene behavior [9,31–37]. The experiments carried out by Lipatov et al. on $Ti_3C_2T_x$ [30] can be replicated with MD to provide a more fundamental understanding of the results. Similarly, a multitude of atomistic indentation studies have been performed on graphene [38–41] with results in good agreement with those from experiment [8]. Modeling MXenes with interatomic potentials presents a challenge due to the number and diversity of different interactions present in a single system; M-M, M-X, X-X, as well as surface terminations and effects. For this reason, a limited number of atomistic studies have been performed on MXenes. One of the approaches taken has been the use of a hybrid style interatomic potential, in which M-M, M-X, and X-X interactions are all modeled independently. Borysiuk et al. have taken this approach to modeling the mechanical behavior of the $Ti_{n+1}C_n$ MXene system with no surface terminations [31,32]. While this approach has yielded results on large scale MXene sheets in good agreement with those predicted via DFT, it is limited to a single MXene system and lacks experimental validation. Another approach to modeling MXenes has been the development of more generalized interatomic potentials. Osti et al. have developed a parameter set for the ReaxFF interatomic potential in order to study the intercalation dynamics of $Ti_3C_2T_x$ MXenes [33]. It is based on the existing TiO_2 parameter set as well as DFT data from the Ti-C interactions in MXenes. The ReaxFF parameter set has not yet been used to study the mechanical properties of MXenes, but if it can successfully model the $Ti_{n+1}C_nT_x$ system including the influence of surface terminations, it could be used for other MXenes as well.

2. Methods

To model indentation on 2D materials with atomistic simulations, a circular region was defined from a larger sheet of monolayer MXene, and atoms within the circular region are free to move while those outside have fixed positions (Fig. 1a). The indenter can be modeled in a variety of ways as long as it remains rigid during indentation and does not bond to the sheet. Some studies have used a Lennard-Jones potential to model indenter-graphene interactions [38,39], but here a simple spherical repulsive force of the following form was used:

$$F(r) = -K(r - r_{tip})^2 \quad (1)$$

where K is a specified force constant, r is the distance from the atom to the center of the indenter, and r_{tip} is the radius of the indenter. In this way, any atom within the sphere of the indenter feels a force, and the indenter will remain rigid so long as K is large enough. A force constant of 3470 nN/nm^2 was used for indentations in this study. Rigidity of the indenter was confirmed by plotting the MXene sheet displacement as a function of indenter position. A linear plot up to the onset of fracture indicated the immediate response of the sheet to coming in contact with the indenter.

The indentation of a 2D material produces a force-displacement curve, which can be modeled within elastic plate theory [8] via the following:

$$F = \sigma_0^{2D}\pi\delta + E^{2D}q^3a^{-2}\delta^3 \quad (2)$$

where a is the radius of the circular hole and q is a function of Poisson's ratio: $q = 1/(1.049–0.15\nu–0.16\nu^2)$ (Fig. 1b). For this study, ν was determined to be 0.291 based on DFT calculations performed on $Ti_3C_2O_2$ [36], however, it should be noted that varying ν within what was deemed a reasonable range for $Ti_3C_2T_x$ MXenes (0.2–0.3) has a minimal effect on Eq. (2). The parameters to be determined via fitting are σ_0^{2D}, which represents the pretension in the film and E^{2D}, a 2D elastic constant related to Young's modulus through the film thickness ($E = E^{2D}/t$). Isotropic mechanical properties can be assumed in this situation due to the sixfold rotational symmetry of the MXene lattice [8]. For consistency, the thickness of each MXene monolayer used in this study was determined as the center-center distance between two T groups aligned along the c-axis plus the diameter of the T group (0.856 nm for $Ti_3C_2O_2$ and 0.614 nm for Ti_2CO_2) (Fig. 1c). For comparison, experimental calculations on monolayer $Ti_3C_2T_x$ assumed a thickness of 0.98 nm, determined via atomically resolved transmission electron microscopy (TEM) [30]. From the force-displacement curve, the breaking strength of the material, σ_{max}^{2D}, can also be determined via the following equation:

$$\sigma_{max}^{2D} = \sqrt{\frac{F_f E^{2D}}{4\pi r_{tip}}} \quad (3)$$

where F_f is the fracture force and r_{tip} is the radius of the spherical indenter (Fig. 1b). The breaking strength represents the intrinsic strength of a 2D material. The fracture force in Eq. (3) was taken as the maximum force up to the point where fits to Eq. (2) were made. Fits were made only within the elastic regime up to the onset of fracture, which was determined by the first deviation from linearity of sheet displacement vs. indenter position plots.

The plate theory model assumes a point-load is applied, i.e., the radius of the indenter tip is significantly smaller than that of the circular hole ($r_{tip}/a < 0.03$). In experiments with indenter tips on the order of nanometers and holes on the order of microns this is a reasonable assumption, however, it is not the case at the nanometer scale of atomistic simulations. As such, Tan et al. proposed a modification to Eq. (2) taking into account a sphere-load, in which the cubic term is corrected by a factor of $(r_{tip}/a)^{1/4}$ [39]. Within this framework, a point-load is assumed initially when the contact area between the indenter and sheet is small, and a sphere-load is used thereafter for large displacements. This sectional fitting approach has been necessary in simulations of graphene indentation as displacements regularly reach values of $\delta/a = 1$ prior to fracture. However, in the current work, the largest displacement observed prior to the onset of failure was only $\delta/a = 0.25$, and therefore the point-load model described in Eq. (2) was used for all fits.

The previously mentioned computational indentation studies [38–41] all investigated 2D materials in the absence of defects. This is a reasonable approach for studying graphene as mechanical exfoliation has the capability of producing such pristine sheets, but the harsh environments of solution processing (usually hydrofluoric acid containing) have been shown to impart defects in MXenes [42]. Additionally, MXenes will inherit defects present in their MAX phase precursors, which have been shown to be rather abundant [43,44]. Defects play a major role in determining the mechanical behavior of all material systems. Therefore, in addition to pristine MXene monolayers, this study examines the effect of randomly introduced Ti (V_{Ti}) and C (V_C) vacancies on MXene mechanical behavior. A random vacancy distribution was chosen as predominantly single, isolated vacancies are observed in MXenes synthesized under mild conditions while vacancy clusters only become prevalent when higher hydrofluoric acid concentrations are used [42]. This gives a better analogue to experimental results [30] and offers a comparison to properties theoretically achievable with pristine materials.

All indentations in this study were performed on 25 nm diameter monolayers with full coverage of -O terminations, typically the dominant surface group [45]. The ReaxFF interatomic potential developed for the $Ti_3C_2T_x$ system [46] was used to model all interactions with a timestep of 0.25 fs. A 10-nm-diameter indenter tip was chosen to mimic the size of experimental AFM indenters while keeping the r_{tip}/a ratio as small as possible. An indentation rate of 10 m/s was used, and the temperature was maintained at 1 K throughout indentation within the canonical (NVT) ensemble. All simulations were implemented within the Large-scale Atomic/Molecular Massively Parallel Simulator (LAMMPS) [47] and atomic imaging was performed in OVITO [48].

3. Results and discussion

The force-displacement curve for a pristine monolayer of $Ti_3C_2O_2$ is shown in Fig. 2a. The initial elastic part of the curve appears to follow Eq. (2) followed by a gradual fracture process. This is in sharp contrast to the behavior observed in graphene, both experimentally [8] and computationally [38–41], which fractures suddenly once the process is initiated. This could be attributed to the additional atomic layers in $Ti_3C_2O_2$ providing added resistance to crack propagation. $Ti_3C_2O_2$ has 7 atomic layers, consisting of 3, 2, and 2 layers of Ti, C, and O respectively. The fit to Eq. (2) provides an E^{2D} value of 399 N/m and a corresponding Young's modulus of 466 GPa. This value of Young's modulus is slightly lower than those calculated via DFT (523 GPa) [9] and hybridized MD (502 GPa) [31], but could be due to the presence of surface terminations, which were not considered in those studies. The Young's modulus calculated here is higher than that calculated experimentally (330 GPa) [30] as would be expected from a pristine sheet. Some of this discrepancy also stems from the difference in assumed MXene flake thickness. If the experimentally determined thickness of 0.98 nm is used, the calculated Young's modulus becomes 407 GPa. Despite being significantly lower than the calculated Young's modulus of graphene, this value is more than double that of graphene oxide, the current standard for solution-processed, 2D materials. Similarly, the calculated breaking strength of 25.2 N/m is significantly lower than that of graphene (42 N/m) [8], but still represents a milestone for solution processed, 2D materials.

Fig. 2b shows the force-displacement curve for a pristine monolayer of Ti_2CO_2, a thinner MXene film which has 5 layers of atoms, 2, 1, and 2 atomic layers of Ti, C, and O respectively. In contrast to $Ti_3C_2O_2$, fracture occurs more suddenly at a higher force and lower displacement. Having 2 less atomic layers in Ti_2CO_2 than $Ti_3C_2O_2$ could explain

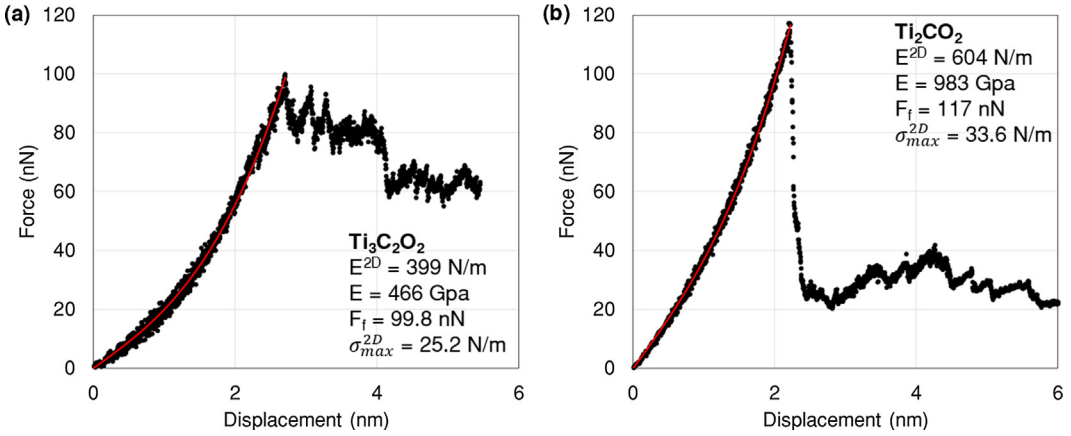

Fig. 2. Force-Displacement curves for pristine monolayers of $Ti_3C_2O_2$ (a) and Ti_2CO_2 (b). Both simulated data (black) and fits to Eq. (2) (red) are shown. Both fits have $R^2 > 0.99$ indicating an appropriate model. (For interpretation of the references to colour in this figure legend, the reader is referred to the web version of this article.)

the more abrupt failure. Fitting the Ti_2CO_2 elastic region to Eq. (2) results in an E^{2D} value of 604 N/m and a Young's modulus of 983 GPa, significantly higher than that calculated for $Ti_3C_2O_2$ and approximately the same as graphene. The calculated breaking strength of 33.6 N/m is also higher than that of $Ti_3C_2O_2$ and approaching the levels of graphene. The calculated Young's modulus for Ti_2CO_2 is not, however, in very good agreement with previously calculated values from DFT (636 GPa) [9] and hybridized MD (597 GPa) [31]. The trend of increasing Young's modulus from $Ti_3C_2T_x$ to Ti_2CT_x is the same, but the ratio E_{Ti2C}/E_{Ti3C2} is approximately 1.2, whereas here it is calculated to be 1.8. As there is not yet experimental data available for this system, it is difficult to conclude the accuracy of values for Ti_2CT_x. Regardless, due to the favorable mechanical properties observed in Ti_2CT_x here and elsewhere, further work in optimizing its synthesis to enable experimental studies is warranted.

The pretension in the films, σ_0^{2D}, was determined to be 5.54 N/m and 10.5 N/m for $Ti_3C_2O_2$ and Ti_2CO_2 respectively. These values are about an order of magnitude larger than those observed experimentally [30], but it is to be expected as σ_0^{2D} has been shown to be directly related to r_{tip}/a [40], which is about an order of magnitude larger in MD indentations as well. The elastic properties are largely independent of σ_0^{2D} as has been demonstrated in previous MD studies of graphene [39,40].

Fig. 3 shows visualizations of the progressive indentation of the pristine $Ti_3C_2O_2$ and Ti_2CO_2 monolayers. Failure in both sheets appears to start with the simultaneous initiation of several cracks near the center (Fig. 3b, f) shortly after the fracture force is reached. In both cases, three cracks are apparent at approximately 120° to one another, consistent with the in-plane symmetry of the hexagonal MXene lattice. As the cracks propagate outward, a triangle-shaped hole appears in the middle of the sheets (Fig. 3d, h). The crack propagation in the thinner Ti_2CO_2 is noticeably faster than in the thicker $Ti_3C_2O_2$ providing evidence for its more rapid failure as discussed above. The cracks appear to be traveling to the edges of the sheets without impedance, an indication of a pristine material lacking defects. Animations of both indentations are provided as supplementary material with additional coloring by atomic strain.

Similar to other materials where defects can strongly influence the fundamental mechanical behavior, MXenes are no exception. Sang et al. recently observed via STEM the presence of V_{Ti} in $Ti_3C_2T_x$ [42]. These defects were observed to be present in concentrations ranging between 1 and 3% and to be dependent upon the concentration of hydrofluoric acid used in the selective etching of MXene synthesis; higher concentrations resulted in a higher defect concentration. Other defects in MXenes include pinholes, and it can be assumed V_C are inherited from the MAX phase precursors as titanium carbides always contain vacancies in the carbon sub-lattice. Several studies have noted the presence of up to 10% V_C in MAX phases such as V_4AlC_3 [43] and Nb_4AlC_3 [44]. Therefore, indentation simulations were repeated on $Ti_3C_2O_2$ monolayers with both V_{Ti} and V_C concentrations ranging between 1 and 10%. The resulting force-displacement curves were fitted with Eq. (2) and the calculated Young's moduli are plotted in Fig. 4 as a function of defect concentration. With the introduction of both defect types, there is a steady decrease in Young's modulus with increasing defect concentration. V_{Ti} appear to cause a more significant reduction across all concentrations. The Young's modulus for sheets containing between 1 and 3% V_{Ti}, the experimentally observed concentrations, range between 410 and 430 GPa. At a 10% concentration of V_{Ti}, the Young's modulus has been reduced from the pristine value of 466 GPa to 316 GPa, a 32.2% decrease. This is similar to the experimentally observed Young's modulus, but it is unlikely that V_{Ti} were present in this high of a concentration based upon the synthesis methods used [30]. A more likely explanation is the presence of multiple types of defects in the experimentally synthesized sheets. At smaller concentrations the introduction of V_C results in little to no change of the Young's modulus. At a 4% concentration of V_C, the Young's modulus begins to decrease with a final value of 375 GPa at 10% concentration. This corresponds to a decrease of 19.5% from the pristine value. As the defects examined here are randomly generated, there would be some variance in the calculated values for Young's modulus if multiple simulations at each concentration were run. Despite this, the general observation that defects have a significant effect on the mechanical properties of $Ti_3C_2O_2$ is evident, and it warrants a more thorough investigation, guided by careful material characterization, of a specific defect composition, which is likely present in real MXene sheets.

A more realistic MXene sheet is likely to contain multiple types of defects, and based on the current synthesis procedure for $Ti_3C_2T_x$ [29] and a non-ideal MAX phase precursor, likely defect concentrations for a $Ti_3C_2O_2$ monolayer used in experiment are about 1% V_{Ti} and 10% V_C. Therefore, these defect concentrations were randomly generated in 10 different samples and indentation simulations were repeated. The force-displacement curve and fit to Eq. (2) are shown for a representative sample in Fig. 5a. After the initial elastic portion of the curve, the onset of fracture begins with a sharp drop in force. However, unlike the pristine sample, the force then begins to rise again above the previous maximum as a gradual fracture process occurs. A possible explanation for this is the impedance of crack propagation by defects. As a crack initiates, the force initially drops, but once it is arrested by defects, the force begins to rise again as it can no longer propagate. This can be seen in the progressive indentation images shown in Fig. 5b–d. Fig. 5b represents the onset of fracture and crack initiation. However, in Fig. 5c, the maximum force achieved, it is clear that the crack has been impeded. The extent of its propagation is much less than that observed in

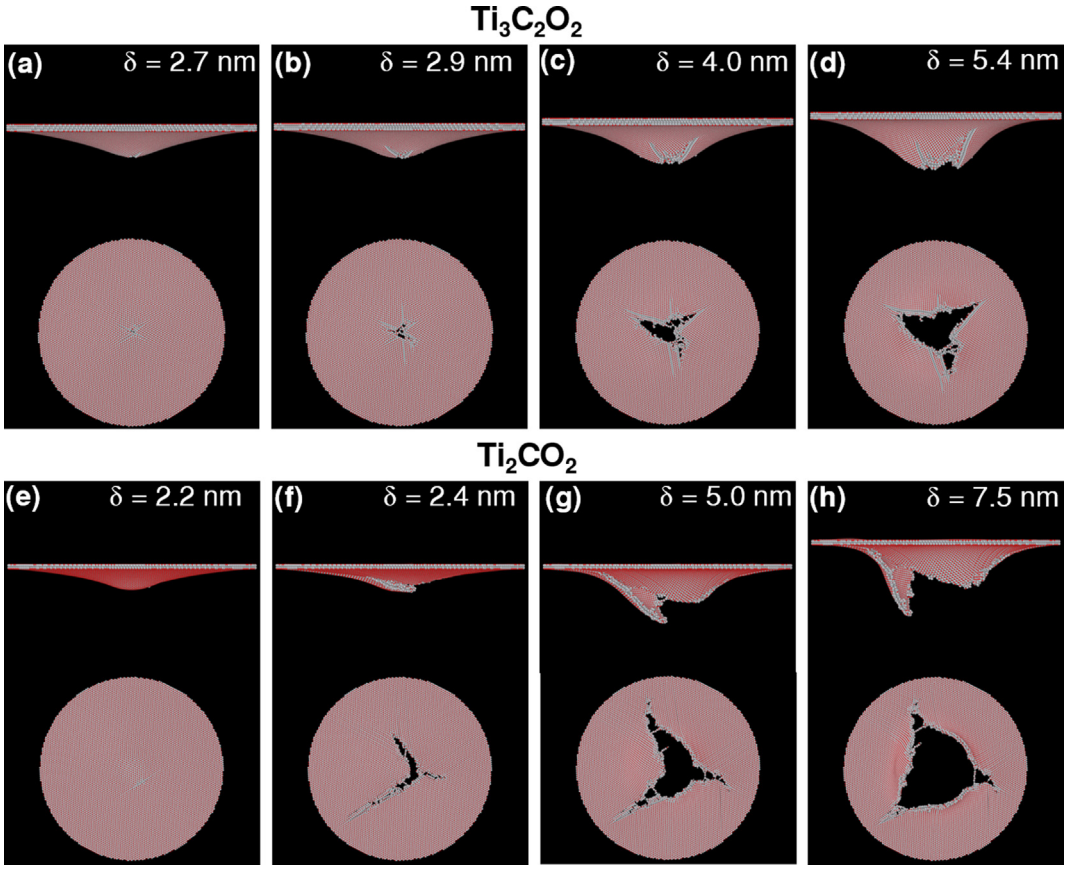

Fig. 3. Images showing the progressive indentation and fracture of pristine monolayers of $Ti_3C_2O_2$ (a–d) and Ti_2CO_2 (e–h). The first images in both series (a, e) represent the point up to which fits were made, i.e. the initiation of fracture. Images are shown along both the a- and c-axes, and atoms are colored according to element.

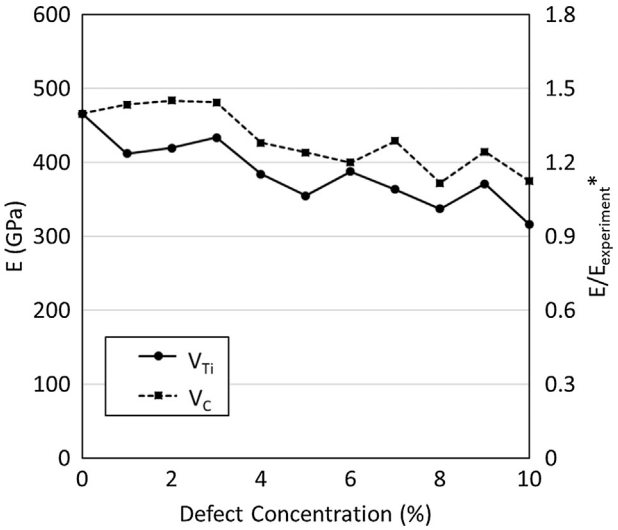

Fig. 4. A plot showing how the Young's modulus of a $Ti_3C_2O_2$ monolayer changes as different concentrations of V_{Ti} and V_C are introduced. *Experimental data from [30].

the pristine sheet (Fig. 3c–d). A hole in the sheet becomes apparent as the force begins to drop (Fig. 5d), but it is contained near the center of the sheet by defects. This explanation is in agreement with the experimental observations of $Ti_3C_2T_x$ indentation as holes were contained to a localized region upon fracture [30] and in contrast to the experimental indentation of pristine graphene, in which holes were observed to propagate over the entire suspended region [8]. An animation of this indentation is provided as supplementary material with additional coloring by atomic strain.

The force-displacement curves from all 10 $Ti_3C_2O_2$ samples were fit with Eq. (2), and both the Young's modulus and breaking strength were calculated. Fig. 6a shows the distribution of calculated Young's moduli. Despite the limited sample size, it appears to be a normal distribution with a mean value of 386 GPa and a standard deviation of 31 GPa. This represents a 17.2% decrease from the pristine value of 466 GPa. The presence of defects would be expected to cause this decrease, but it is not overly significant for the high concentrations implemented and remains above the 200 GPa standard of graphene oxide. Fig. 6b shows the distribution of calculated breaking strengths. It also appears to be somewhat normal with a mean value of 22.0 N/m and a standard deviation of 0.8 N/m. This represents a 12.7% decrease from the 25.2 N/m breaking strength of pristine $Ti_3C_2O_2$, again expected, but not overly significant. The reduced values for Young's modulus and breaking strength calculated here for defective $Ti_3C_2O_2$ samples approach those measured experimentally (330 GPa and 17.0 N/m respectively) [30]. Since the defect concentrations used here were likely present in the experimentally tested sheets, this provides compelling evidence that defects such as V_{Ti} and V_C were responsible for much of the observed elastic behavior and its deviation from previous computational studies. It should be noted that the mean value of E^{2D} from these 10 samples is 330 N/m, in remarkably good agreement with the mean value from experiment of 326 N/m [30]. The discrepancy in the Young's modulus noted above arises from the assumed MXene flake thickness used in its calculation. When the experimentally determined $Ti_3C_2T_x$ thickness of 0.98 nm is applied, the mean Young's modulus becomes 337 GPa, similar to the experimental value of 330 GPa. Despite the impact defects have been shown to have on MXene behavior, this data provides a

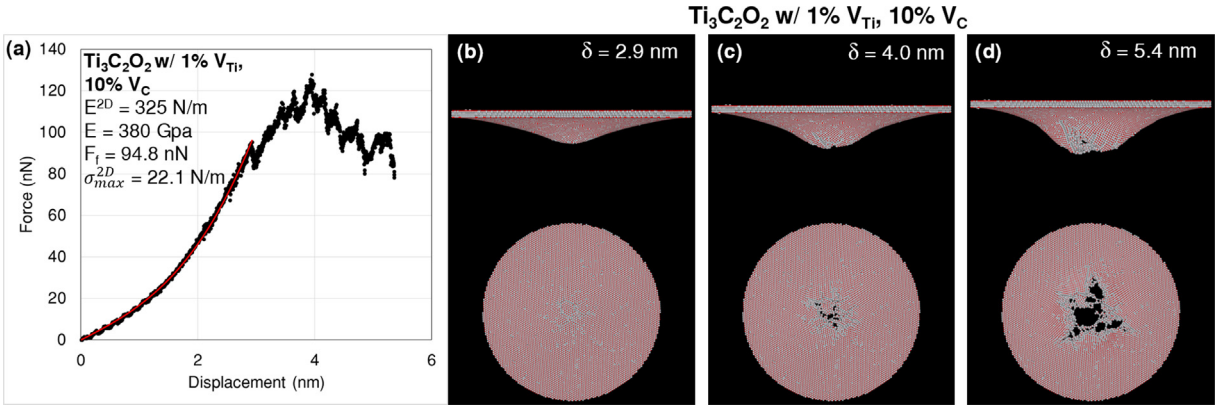

Fig. 5. (a) A representative force-displacement curve. Both simulated data (black) and fits to Eq. (2) (red) are shown. All 10 fits have $R^2 > 0.99$ indicating an appropriate model. (b-d) Images showing the progressive indentation and fracture of the same representative $Ti_3C_2O_2$ monolayer with 1% V_{Ti} and 10% V_C. The first image (b) represents the point up to which a fit was made, i.e. the initiation of fracture. Images are shown along both the a- and c-axes, and atoms are colored according to element. (For interpretation of the references to colour in this figure legend, the reader is referred to the web version of this article.)

promising outlook for the mechanical properties of real $Ti_3C_2O_2$ sheets. They are not significantly reduced from the theoretical pristine values and remain a benchmark for solution-processed, 2D materials. Experimental measurements confirm that these properties can be achieved with current synthesis methods.

4. Conclusions

Prediction of MXene mechanical strength makes them exciting candidates for incorporation into composites for wide-ranging applications such as structural components, energy storage devices, flexible electronics, membranes, etc. As demonstrated here, atomistic simulations can serve as an important tool in providing insight and further understanding of the mechanical behavior of MXenes. Indentations were performed on both $Ti_3C_2O_2$ and Ti_2CO_2 MXenes, and properties were extracted by fitting the force-displacement curves with elastic plate theory. $Ti_3C_2O_2$ and Ti_2CO_2 were calculated to have Young's moduli of 466 GPa and 983 GPa respectively, greater than that of graphene oxide, the current standard for solution processed, 2D materials. A set of "realistic" $Ti_3C_2O_2$ samples containing both V_{Ti} and V_C were created and indentation simulations repeated. The defects had a clear effect on the fracture mechanism of the sheets as cracks failed to propagate all the way to the edges as they had in the pristine sheet. The mean Young's modulus from the 10 samples only decreased 17.2% from the pristine value to 386 GPa, remaining above that of graphene oxide. These results are in good agreement with recent experimental measurements [30] and provide further insight into how defects influence MXene mechanical properties. It is clear that despite the presence of defects, with current processing methods, $Ti_3C_2T_x$ MXenes can become the new standard for mechanical properties in solution-processed, 2D materials.

CRediT authorship contribution statement

Gabriel Plummer: Conceptualization, Methodology, Data curation, Formal analysis, Investigation, Writing – original draft. **Babak Anasori:** Conceptualization, Supervision, Writing – review & editing. **Yury Gogotsi:** Conceptualization, Supervision, Writing – review & editing. **Garritt J. Tucker:** Conceptualization, Methodology, Supervision, Writing – review & editing.

Acknowledgements

Work reported here was run on hardware supported by Drexel's University Research Computing Facility. This work was partially supported by the National Science Foundation under Grant No. 1728041. G.P. was supported, in part, by a graduate research fellowship funded by CoorsTek Inc. B.A. and Y.G. were supported by U.S. Army Research Office grant W911NF-17-2-0228. The authors thank Dr. A. van Duin for providing the ReaxFF parametrization used herein. The authors declare that they have no competing interests.

Data availability

The data required to reproduce these findings are available upon request.

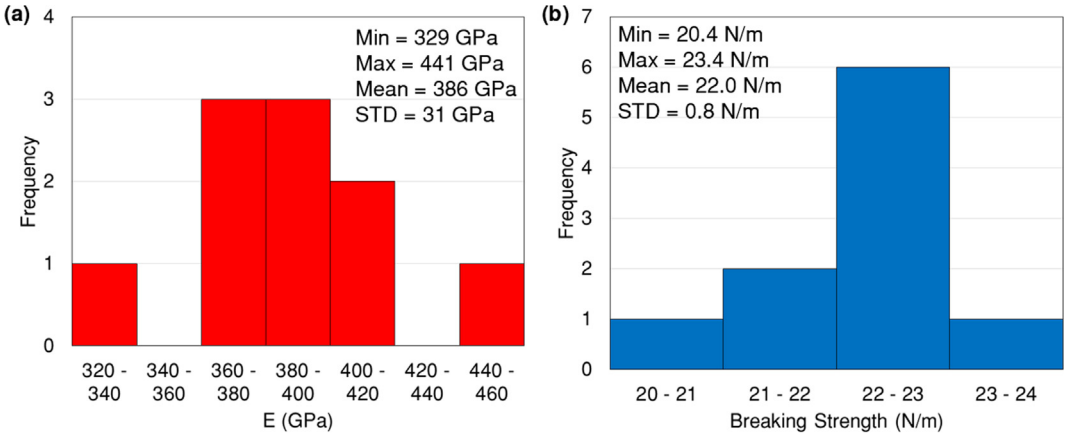

Fig. 6. (a) A distribution of the calculated Young's moduli for all 10 samples. (b) A distribution of the calculated breaking strengths for all 10 samples.

Appendix A. Supplementary material

Supplementary data to this article can be found online at https://doi.org/10.1016/j.commatsci.2018.10.033.

References

[1] M. Naguib, M. Kurtoglu, V. Presser, J. Lu, J. Niu, M. Heon, L. Hultman, Y. Gogotsi, M.W. Barsoum, Two-dimensional nanocrystals produced by exfoliation of Ti_3AlC_2, Adv. Mater. 23 (2011) 4248–4253.

[2] B. Anasori, M.R. Lukatskaya, Y. Gogotsi, 2D metal carbides and nitrides (MXenes) for energy storage, Nat. Rev. Mater. 2 (2017) 16098.

[3] M.W. Barsoum, MAX Phases: Properties of Machinable Ternary Carbides and Nitrides, John Wiley & Sons, 2013.

[4] M. Dahlqvist, J. Lu, R. Meshkian, Q. Tao, L. Hultman, J. Rosen, Prediction and synthesis of a family of atomic laminate phases with Kagomé-like and in-plane chemical ordering, Sci. Adv. 3 (2017) e1700642.

[5] M. Naguib, V.N. Mochalin, M.W. Barsoum, Y. Gogotsi, 25th anniversary article: MXenes: a new family of two-dimensional materials, Adv. Mater. 26 (2014) 992–1005.

[6] M.R. Lukatskaya, S. Kota, Z. Lin, M.-Q. Zhao, N. Shpigel, M.D. Levi, J. Halim, P.-L. Taberna, M.W. Barsoum, P. Simon, Y. Gogotsi, Ultra-high-rate pseudocapacitive energy storage in two-dimensional transition metal carbides, Nat. Energy 2 (2017) 17105.

[7] F. Shahzad, M. Alhabeb, C.B. Hatter, B. Anasori, S. Man Hong, C.M. Koo, Y. Gogotsi, Electromagnetic interference shielding with 2D transition metal carbides (MXenes), Science 353 (2016) 1137.

[8] C. Lee, X. Wei, J.W. Kysar, J. Hone, Measurement of the elastic properties and intrinsic strength of monolayer graphene, Science 321 (2008) 385–388.

[9] M. Kurtoglu, M. Naguib, Y. Gogotsi, M.W. Barsoum, First principles study of two-dimensional early transition metal carbides, MRS Commun. 2 (2012) 133–137.

[10] M. Yi, Z. Shen, A review on mechanical exfoliation for the scalable production of graphene, J. Mater. Chem. A 3 (2015) 11700–11715.

[11] Z. Ling, C.E. Ren, M.-Q. Zhao, J. Yang, J.M. Giammarco, J. Qiu, M.W. Barsoum, Y. Gogotsi, Flexible and conductive MXene films and nanocomposites with high capacitance, Proc. Natl. Acad. Sci. 111 (2014) 16676–16681.

[12] M. Boota, B. Anasori, C. Voigt, M.Q. Zhao, M.W. Barsoum, Y. Gogotsi, Pseudocapacitive electrodes produced by oxidant-free polymerization of pyrrole between the layers of 2D titanium carbide (MXene), Adv. Mater. 28 (2015) 1517–1522.

[13] C. Chen, M. Boota, X. Xie, M. Zhao, B. Anasori, C.E. Ren, L. Miao, J. Jiang, Y. Gogotsi, Charge transfer induced polymerization of EDOT confined between 2D titanium carbide layers, J. Mater. Chem. A 5 (2017) 5260–5265.

[14] M. Alhabeb, K. Maleski, B. Anasori, P. Lelyukh, L. Clark, S. Sin, Y. Gogotsi, Guidelines for synthesis and processing of two-dimensional titanium carbide ($Ti_3C_2T_x$ MXene), Chem. Mater. 29 (2017) 7633–7644.

[15] J.W. Suk, R.D. Piner, J. An, R.S. Ruoff, Mechanical properties of monolayer graphene oxide, ACS Nano 4 (2010) 6557–6564.

[16] H. Zhang, L. Wang, Q. Chen, P. Li, A. Zhou, X. Cao, Q. Hu, Preparation, mechanical and anti-friction performance of MXene/polymer composites, Mater. Des. 92 (2016) 682–689.

[17] W.H. Woodford, Y.-M. Chiang, W.C. Carter, "Electrochemical shock" of intercalation electrodes: a fracture mechanics analysis, J. Electrochem. Soc. 157 (2010) A1052–A1059.

[18] M.Q. Zhao, E. Ren Chang, Z. Ling, R. Lukatskaya Maria, C. Zhang, L. Van Aken Katherine, W. Barsoum Michel, Y. Gogotsi, Flexible MXene/carbon nanotube composite paper with high volumetric capacitance, Adv. Mater. 27 (2015) 339–345.

[19] Z. Zhou, W. Panatdasirisuk, T.S. Mathis, B. Anasori, C. Lu, X. Zhang, Z. Liao, Y. Gogotsi, S. Yang, Layer-by-layer assembly of MXene and carbon nanotubes on electrospun polymer films for flexible energy storage, Nanoscale 10 (2018) 6005–6013.

[20] C.E. Ren, K.B. Hatzell, M. Alhabeb, Z. Ling, K.A. Mahmoud, Y. Gogotsi, Charge- and size-selective ion sieving through $Ti_3C_2T_x$ MXene membranes, J. Phys. Chem. Lett. 6 (2015) 4026–4031.

[21] L. Ding, Y. Wei, Y. Wang, H. Chen, J. Caro, H. Wang, A two-dimensional lamellar membrane: MXene nanosheet stacks, Angew. Chem. Int. Ed. 56 (2017) 1825–1829.

[22] R.P. Pandey, K. Rasool, E. Vinod, B. Aissa, Y. Gogotsi, K.A. Mahmoud, Ultrahigh-flux and fouling-resistant membrane based on layered silver/MXene ($Ti_3C_2T_x$) nanosheets, J. Mater. Chem. A 6 (2018) 3522–3533.

[23] J. Wang, P. Chen, B. Shi, W. Guo, M. Jaroniec, S.Z. Qiao, A Regularly Channeled lamellar membrane for unparalleled water and organics permeation, Angew. Chem. 57 (2018) 6814–6818.

[24] L. Ding, Y. Wei, L. Li, T. Zhang, H. Wang, J. Xue, L.-X. Ding, S. Wang, J. Caro, Y. Gogotsi, MXene molecular sieving membranes for highly efficient gas separation, Nat. Commun. 9 (2018) 155.

[25] Y. Ma, N. Liu, L. Li, X. Hu, Z. Zou, J. Wang, S. Luo, Y. Gao, A highly flexible and sensitive piezoresistive sensor based on MXene with greatly changed interlayer distances, Nat. Commun. 8 (2017) 1207.

[26] Y. Cai, J. Shen, G. Ge, Y. Zhang, W. Jin, W. Huang, J. Shao, J. Yang, X. Dong, Stretchable $Ti_3C_2T_x$ MXene/carbon nanotube composite based strain sensor with ultrahigh sensitivity and tunable sensing range, ACS Nano 12 (2018) 56–62.

[27] A. Falin, Q. Cai, E.J. Santos, D. Scullion, D. Qian, R. Zhang, Z. Yang, S. Huang, K. Watanabe, T. Taniguchi, Mechanical properties of atomically thin boron nitride and the role of interlayer interactions, Nat. Commun. 8 (2017) 15815.

[28] S. Bertolazzi, J. Brivio, A. Kis, Stretching and breaking of ultrathin MoS_2, ACS Nano 5 (2011) 9703–9709.

[29] A. Lipatov, M. Alhabeb, M.R. Lukatskaya, A. Boson, Y. Gogotsi, A. Sinitskii, Effect of synthesis on quality, electronic properties and environmental stability of individual monolayer Ti_3C_2 MXene flakes, Adv. Electron. Mater. 2 (2016) 1600255.

[30] A. Lipatov, H. Lu, M. Alhabeb, B. Anasori, A. Gruverman, Y. Gogotsi, A. Sinitskii, Elastic properties of 2D $Ti_3C_2T_x$ MXene monolayers and bilayers, Sci. Adv. 4 (2018) eeat0491.

[31] V.N. Borysiuk, V.N. Mochalin, Y. Gogotsi, Molecular dynamic study of the mechanical properties of two-dimensional titanium carbides $Ti_{n+1}C_n$ (MXenes), Nanotechnology 26 (2015) 265705.

[32] V.N. Borysiuk, V.N. Mochalin, Y. Gogotsi, Bending rigidity of two-dimensional titanium carbide (MXene) nanoribbons: a molecular dynamics study, Comput. Mater. Sci. 143 (2018) 418–424.

[33] N.C. Osti, M. Naguib, A. Ostadhossein, Y. Xie, P.R. Kent, B. Dyatkin, G. Rother, W.T. Heller, A.C. van Duin, Y. Gogotsi, Effect of metal ion intercalation on the structure of MXene and water dynamics on its internal surfaces, ACS Appl. Mater. Interfaces 8 (2016) 8859–8863.

[34] Y. Xie, Y. DallAgnese, M. Naguib, Y. Gogotsi, M.W. Barsoum, H.L. Zhuang, P.R.C. Kent, Prediction and characterization of MXene nanosheet anodes for non-lithium-ion batteries, ACS Nano 8 (2014) 9606–9615.

[35] Y. Xie, M. Naguib, V.N. Mochalin, M.W. Barsoum, Y. Gogotsi, X. Yu, K.-W. Nam, X.-Q. Yang, A.I. Kolesnikov, P.R.C. Kent, Role of surface structure on Li-ion energy storage capacity of two-dimensional transition-metal carbides, J. Am. Chem. Soc. 136 (2014) 6385–6394.

[36] Z. Fu, Q. Zhang, D. Legut, C. Si, T. Germann, T. Lookman, S. Du, J. Francisco, R. Zhang, Stabilization and strengthening effects of functional groups in two-dimensional titanium carbide, Phys. Rev. B 94 (2016) 104103.

[37] T. Hu, H. Zhang, J. Wang, Z. Li, M. Hu, J. Tan, P. Hou, F. Li, X. Wang, Anisotropic electronic conduction in stacked two-dimensional titanium carbide, Sci. Rep. 5 (2015) 16329.

[38] M. Neek-Amal, F. Peeters, Nanoindentation of a circular sheet of bilayer graphene, Phys. Rev. B 81 (2010) 235421.

[39] X. Tan, J. Wu, K. Zhang, X. Peng, L. Sun, J. Zhong, Nanoindentation models and Young's modulus of monolayer graphene: a molecular dynamics study, Appl. Phys. Lett. 102 (2013) 071908.

[40] W. Wang, S. Li, J. Min, C. Yi, Y. Zhan, M. Li, Nanoindentation experiments for single-layer rectangular graphene films: a molecular dynamics study, Nanoscale Res. Lett. 9 (2014) 41.

[41] M. Huang, T.A. Pascal, H. Kim, W.A. Goddard III, J.R. Greer, Electronic − mechanical coupling in graphene from in situ nanoindentation experiments and multiscale atomistic simulations, Nano Lett. 11 (2011) 1241–1246.

[42] X. Sang, Y. Xie, M.-W. Lin, M. Alhabeb, K.L. Van Aken, Y. Gogotsi, P.R. Kent, K. Xiao, R.R. Unocic, Atomic defects in monolayer titanium carbide ($Ti_3C_2T_x$) MXene, ACS Nano 10 (2016) 9193–9200.

[43] J. Etzkorn, M. Ade, H. Hillebrecht, V_2AlC, V_4AlC_{3-x} ($x \approx 0.31$), and $V_{12}Al_3C_8$: Synthesis, crystal growth, structure, and superstructure, Inorg. Chem. 46 (2007) 7646–7653.

[44] H. Zhang, T. Hu, X. Wang, Z. Li, M. Hu, E. Wu, Y. Zhou, Discovery of carbon-vacancy ordering in Nb_4AlC_{3-x} under the guidance of first-principles calculations, Sci. Rep. 5 (2015) 14192.

[45] J. Halim, K.M. Cook, M. Naguib, P. Eklund, Y. Gogotsi, J. Rosen, M.W. Barsoum, X-ray photoelectron spectroscopy of select multi-layered transition metal carbides (MXenes), Appl. Surf. Sci. 362 (2016) 406–417.

[46] Van Duin AC. The ReaxFF parametrization used herein is available by request: https://www.mri.psu.edu/materials-computation-center/connect-mcc. Private Communication.

[47] S. Plimpton, Fast parallel algorithms for short-range molecular dynamics, J. Comput. Phys. 117 (1995) 1–19.

[48] A. Stukowski, Visualization and analysis of atomistic simulation data with OVITO–the Open Visualization Tool, Modell. Simul. Mater. Sci. Eng. 18 (2009) 015012.